Mon. Not. R. astr. Soc. (1987) **226,** 785–811

Spin-up and spin-down of an accreting compact object

Takuya Matsuda, Minoru Inoue and Keisuke Sawada*
Department of Aeronautical Engineering, Kyoto University, Kyoto 606, Japan

Accepted 1986 November 5. Received 1986 October 24; in original form 1986 July 21

Summary. Two-dimensional hydrodynamic calculations of an accretion flow on to a compact object fed by a stellar wind in a close binary system with a mass ratio of unity are performed. We consider the case in which a stellar wind is driven by a thermal pressure. The parameters specifying the problem are the sound speed of gas, c_0, at the surface of the mass-losing star and the ratio of specific heats, γ.

In the case of $\gamma=5/3$, it is found that the flow is rather unstable when $c_0=1.0$–1.4, and a unique solution is not found. In the case of $c_0=1.5$, we found a retrograde rotating accretion disc separated by a bow shock from a wind. In cases of $c_0>=2.0$, we have a conical accretion shock. In the cases of $\gamma=4/3$, we have a conical accretion shock if $c_0>=1.2$. In some models a flow changes its pattern sporadically, and we term it a flip–flop flow.

Time histories of a mass accretion rate and an angular momentum accretion rate on to the compact object are monitored. Their behaviour is not steady generally. The accreted angular momentum flux becomes negative in some models. In the flip–flop flow, the angular momentum accreted by the compact object changes it sign sporadically. This phenomenon is consistent with the random-walk model of a period fluctuation of Vela X-1 and 4U1538−52.

1 Introduction

A substantial fraction of X-ray sources in binary systems are known to exhibit regular X-ray pulsations. They are called X-ray pulsars and are believed to be rotating, magnetized neutron stars. In these interacting binary systems, matter with angular momentum flows from a companion star towards the rotating neutron star, the response of which is the change of its rotation rate, i.e. a spin-up or a spin-down of the neutron star.

Five X-ray pulsars among some 20 presently known ones show a more-or-less steady spin-up (Henrichs 1983). The spin-up behaviour has been generally understood in terms of the torque exerted by an accretion disc formed in a Roche lobe overflow.

Other sources show spin-up and spin-down behaviour. Even for five sources exhibiting a clear

* Aircraft Engineering Division, Kawasaki Heavy Industries Ltd., Kakamigahara 504, Japan.

spin-up trend, the change in pulse period is not always monotonic on short time-scales (Rappaport & Joss 1983).

Vela X-1 (4U0900−40) particularly shows a spin-down after a spin-up period (Nagase 1981; Nagase *et al.* 1984). An average spin-up rate is $\dot{P}/P=-1.5\times10^{-4}\,\mathrm{yr}^{-1}$, while the spin-down rate is $\dot{P}/P=2.6\times10^{-3}\,\mathrm{yr}^{-1}$. Furthermore, Vela X-1 shows fluctuations in the pulse period within the time-scale of an orbital period superimposed on the secular trend of pulse period change. The value of $\dot{P}$ fluctuates between $\dot{P}/P=4\times10^{-3}$ and $-3\times10^{-3}\,\mathrm{yr}^{-1}$ (Nagase *et al.* 1984).

Makishima *et al.* (1986) observed 4U1538−52 and reported that its pulsation period changes in a random-walk manner, which is very similar to Vela X-1.

Such a behaviour is difficult to understand in terms of a simple Roche lobe overflow model. These sources are most likely to be undergoing accretion from a stellar wind. Nagase *et al.* (1984) interpreted the observed pulse-period change as a random-walk process, in response to random polarity reversals in external torque exerted by the stellar wind to the neutron star. The reversals seem to occur on time-scales comparable to the orbital period. Boynton *et al.* (1984) formulated the same idea. Makishima *et al.* (1986) supported this idea on the basis of their observation.

Let us overview accretion theories proposed so far. Davidson & Ostriker (1973) assumed that the net angular momentum with respect to the neutron star of all gas entering the cylindrical volume with an accretion radius r_a is accreted by the neutron star. Here the accretion radius is defined as

$$r_a=2Gm/(V^2+c_s^2), \tag{1.1}$$

where m, V and c_s are the mass of the neutron star, the wind speed and the sound speed of gas, respectively.

The velocity vector of a wind particle makes an angle with respect to the line connecting the mass-losing star and the neutron star. Assuming the stellar wind to be spherically symmetric, there exists a density gradient in the stellar wind across the accretion cross-section. Therefore, the target face will capture different amounts of particles at the far-side and at the near-side. Considering these, Shapiro & Lightman (1979) gave a formula for the captured specific angular momentum, l:

$$l=\tfrac{1}{2}\Omega r_a^2\eta, \tag{1.2}$$

where Ω is the orbital angular velocity and η is an efficiency of the angular momentum accretion. The efficiency factor η is unity if the wind velocity is assumed constant. An essential point in the above theory is that η can never become negative.

In the presence of a radial velocity gradient, the value of η is (Wang 1981)

$$\eta\sim1+7/4(A/R_*-1), \tag{1.3}$$

where A and R_* are the separation of two stars and the radius of the mass-losing star, respectively. In our case $R_*=A/2$, and therefore $\eta=2.75$. Wang (1981) argued that η can become negative if there is significant azimuthal anisotropy in the stellar wind density and/or velocity. However, such a situation seems to be rather unrealistic in X-ray binaries (Masai 1984, private communication).

On the other hand Davies & Pringle (1980) showed that the net accreted angular momentum should be zero in order for any accretion to occur, irrespective of the existence of a density/or velocity gradient across the target face. This result is based on the asumptions: (i) that the accreting star is point like; (ii) that the accretion line joins the point mass; (iii) that no dissipation occurs as the particles stream along the accretion line.

Livio *et al.* (1986) and Soker *et al.* (1986) confirmed this conclusion by the numerical simulations of three-dimensional inhomogeneous accretion. Anzer, Börner & Monaghan (1986)

performed two-dimensional calculations and obtained a similar conclusion. These authors used the smoothed particle hydrodynamics (SPH) technique proposed by Gingold & Monaghan (1983).

None of the theories described above can account for the spin-down phenomena of a neutron star except for a very unrealistic situation, since the specific angular momentum accreted by a compact object is generally positive or zero. Even if the accreted angular momentum were negative, a steady solution could not account for the random-walk model of the spin-up/down of neutron stars described before. Taking this into consideration, it is interesting to see if more realistic calculations can predict unsteady solutions exhibiting both positive and negative angular momentum captured by a neutron star.

The purpose of the present paper is to perform 2D hydrodynamic calculations of wind-fed accretion on to a compact object in order to estimate the amount of angular momentum accreted by it. We compute rather low Mach number cases in order to make the point clear.

Numerical simulations of a stellar wind in a close binary system has been performed by Biermann (1971) and Sorensen, Matsuda & Sakurai (1975), although they did not compute the amount of angular momentum transfer. Recently, we (Sawada, Matsuda & Hachisu 1986b, Paper 1 hereafter) performed numerical simulations on wind-fed accretion and obtained flow patterns using a modern technique of computational hydrodynamics. In the work we actually observed the amount of angular momentum transfer, but we were disappointed to find that no systematic trend in the accreted angular momentum was obtained.

In the present paper, we re-attack the problem using a finer mesh spacing, a sophisticated grid system, a faster computer, a longer computation time and more careful parameter search. We report here quite unexpected results: η can become negative even without the assumption of azimuthal anisotropies in the stellar wind density and/or velocity. Therefore, our result is different from the theories of Shapiro & Lightman (1976), Wang (1981) as well as Davies & Pringle (1980). Moreover, solutions are generally unsteady and the accreted angular momentum changes its sign in a random manner, although the boundary condition on the mass-losing star is kept constant in time.

2 Assumptions

In a case of wind-fed accretion, a mass-losing star need not fulfil its own critical Roche lobe and its mass is generally much larger than a mass-accreting neutron star. In spite of this, we consider a semi-detached binary system of mass-ratio unity in order to make the condition the same as in Paper 1. Therefore, it may not be appropriate to compare our model directly with, say, Vela X-1. Nevertheless, we believe that the results are not heavily dependent on this assumption as far as a basic hydrodynamic behaviour of an accretion flow is concerned.

We restrict our attention to within a thin disc with a constant thickness on the rotational plane in order to make the calculation two dimensional. Three-dimensional calculations will be performed in a near future.

We neglect cooling, heating, viscosity, magnetic fields and radiation. The gas is assumed to be an ideal one with the specific heat ratio γ. We solve a 2D Euler equation with a time-marching method. At an initial stage, uniform tenuous atmosphere is assumed to fill all over the computational domain except inside the stars. Gas begins to be ejected perpendicularly to the surface of the mass-losing star at $t=0$.

We followed the time evolution of the system over a sufficient period. Since the method of solution is the explicit Osher upwind scheme, second-order accurate in space and in time, we can obtain an unsteady solution as well as a steady one. The scheme is described separately (Sawada *et al.* 1986c).

The grid systems used in the present calculation are of multi-box or multi-zone types, which were used in our previous paper (Sawada *et al.* 1987). In order to check the result, we use two grids having different sizes and different numbers of meshes (see Fig. 1). The smaller one (grid A) has 73 circumferential grids and 38 radial ones, while the larger one (grid B) is a 73×48 grid. The radius of the mass-accreting object is set to be $0.01A$, where A is the separation of two stars. In a typical condition this size is comparable to one of a white dwarf or a magneto-sphere of a neutron star with a magnetic field, $B \sim 10^{12}$G.

As to the boundary condition on the mass-losing star, the density, the sound speed and the velocity of gas just inside the surface are specified. Since the density can be normalized by the density mentioned above, we take the above density to be unity. The velocity is set to be zero; this

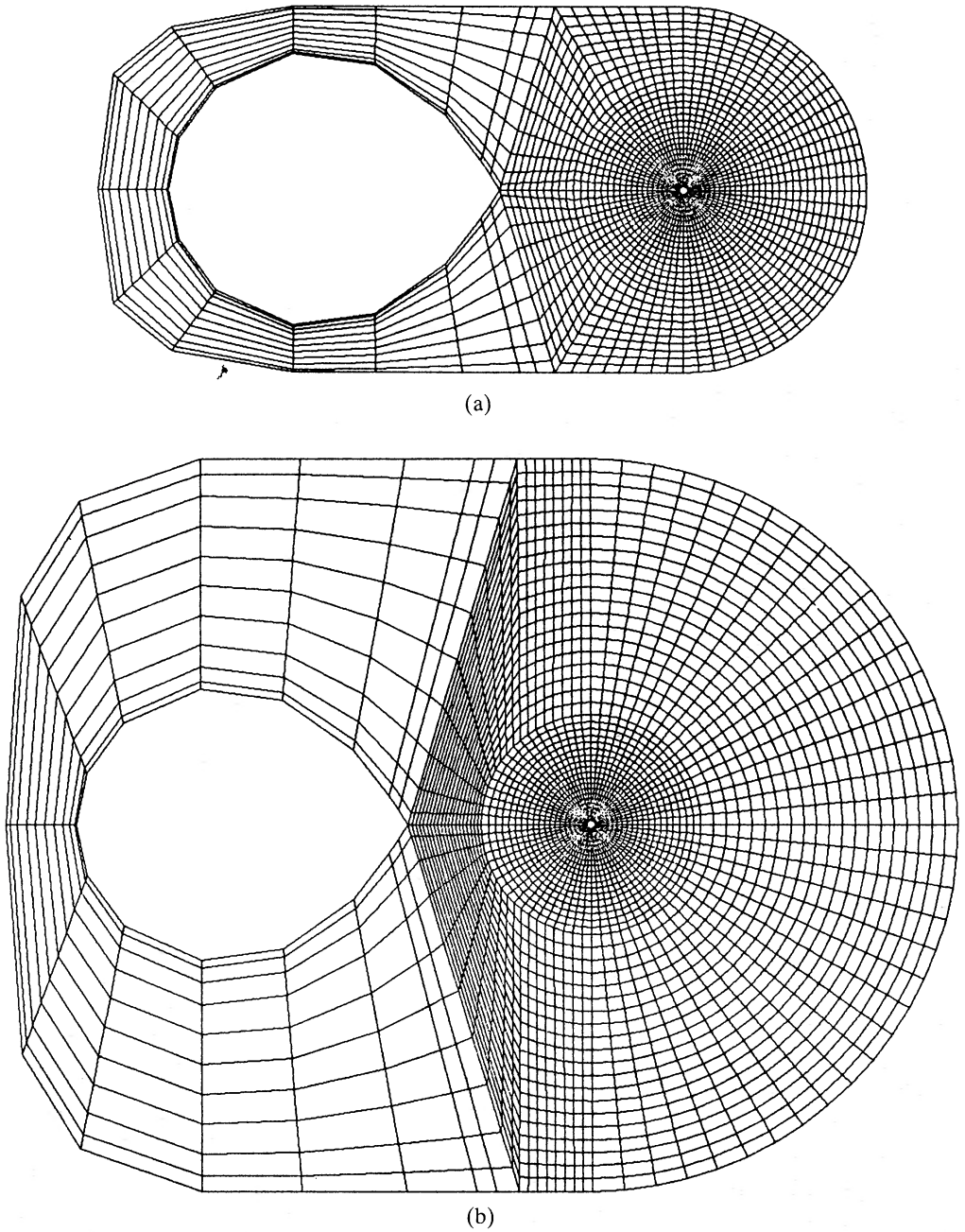

Figure 1. (a). The smaller multi-box type grid used in the present calculation (grid A) having 73×38 meshes. (b) The larger grid (grid B) having 73×48 meshes.

was assumed to be 0.0125 in Paper 1. We are considering, therefore, a thermally driven wind such as the solar wind rather than a radiation driven wind. If we fix the sound speed and vary the velocity of ejected gas, we may simulate a series of solutions corresponding to the radiation driven wind. We meet some numerical difficulty in such a case, and we restrict ourselves here to the thermally driven wind.

The boundary condition on the surface of the mass-losing star can be computed by solving a Riemann problem between the state just inside the surface and that just outside. Parameters specifying the present problem, therefore, are the sound speed of gas c_0 and γ. We will normalize the velocity by $A\Omega$.

At the interior points of the compact object, the density and the pressure of gas is set to be so low that all the gas arriving on the surface of the mass-accreting star is swallowed. At the outer boundary, a similar condition is assumed.

We computed the cases with c_0=1.0, 1.2, 1.3, 1.4, 1.5, 2.0, 2.5, 5.0, and γ=5/3 and 4/3. In Paper 1, we examined only cases with c_0=1.0 and 2.5 with γ=5/3. Assuming the system velocity $A\Omega$=100 km s^{-1} as an example, the above sound speeds correspond to a temperature of 10^6–2.5×10^7 K.

3 Numerical results

Here we describe the cases for γ=5/3 first. When c_0=1.0–1.4, puzzling phenomena occur and these cases will be discussed later. All calculations described in the following three subsections are performed both on grid A and on grid B, and essentially the same results are obtained.

3.1 RETROGRADE-ROTATING DISC

In the case of c_0=1.5, we obtained flow patterns represented in Fig. 2, which shows the density contours and the Mach number contours at t=19 and 20, respectively. They are computed on grid B. The accretion disc about the compact object is rotating clockwise: a retrograde-rotating disc. The accreted angular momentum is negative.

A bow shock detached from the compact object is observed. The flow pattern is not completely steady. Weak shocks (or pressure waves) are formed close to the compact object, and they propagate upstream to merge into the bow shock, which is itself steady.

In order to show that the present result does not depend on the particular choice of an initial condition, we performed an experiment. At first we fixed c_0 to be 0.75 to obtain a Roche lobe overflow. At t=6, we changed c_0 from 0.75 to 1.5 to study further evolution. We obtained a retrograde-rotating disc identical to the previous result shortly after the change, and this pattern persisted up to t=20.

3.2 A SHOCK SHOWING FLIP–FLOP BEHAVIOUR

When we raise c_0 further to 2.0 we obtain an unsteady accretion shock as shown in Fig. 3, which shows flow patterns at t=10, 11 and 12.

At t=10 and 11 the shock is detached from the compact object and a small accretion disc seems to be formed about the compact object. A disc at t=11 possesses a tiny spiral. The sense of rotation of the accretion discs and the direction of the bow shocks are different from time to time. The flow pattern shows such flip–flop behaviour all the time. It is noted that a sonic line surrounding the compact object is closed and therefore effects originating in the outer boundary do not disturb these flow patterns.

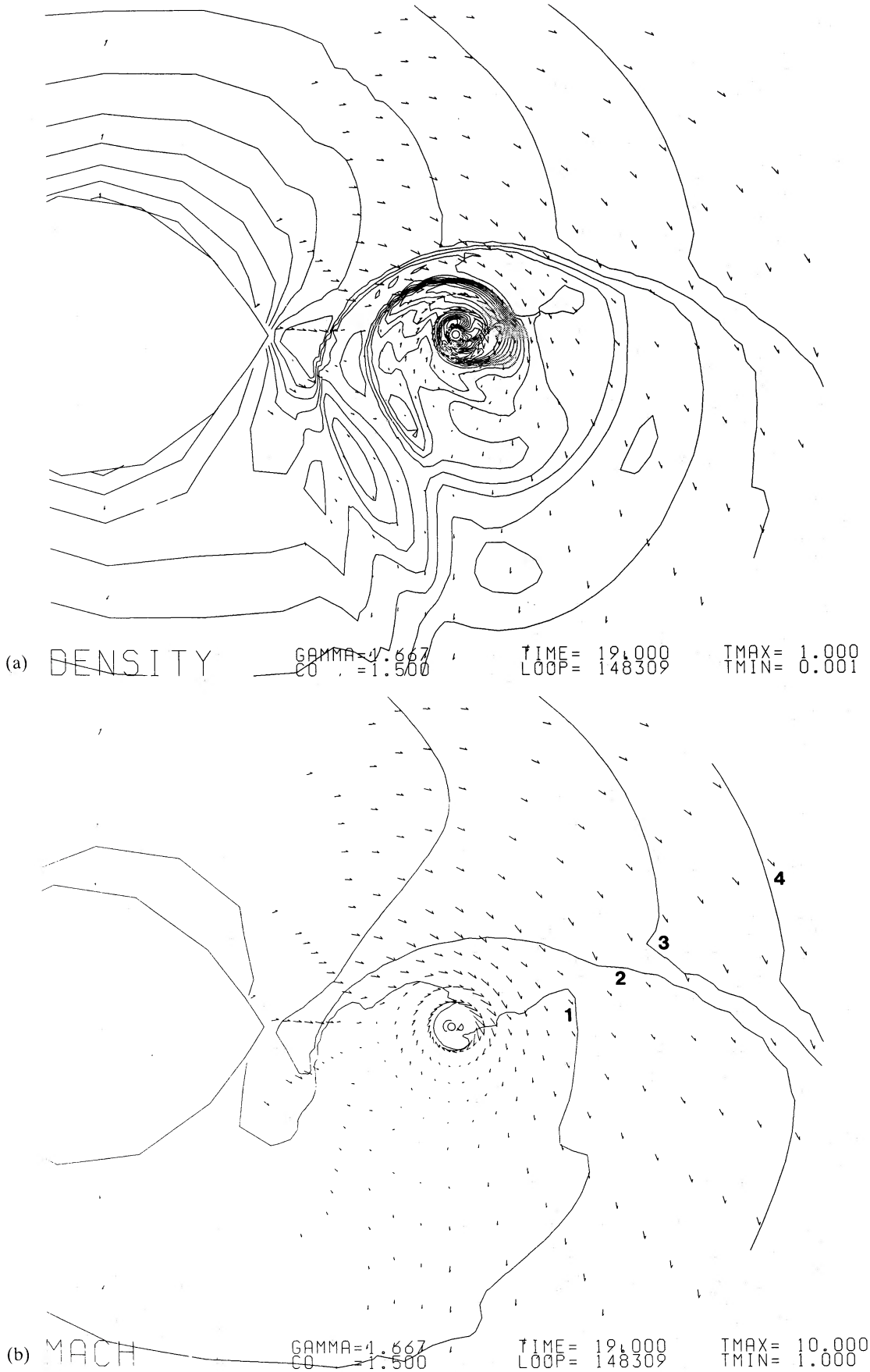

Figure 2. (a) Density contours of the model with $c_0=1.5$ and $\gamma=5/3$ at $t=19$. The density range is from 0.001 to 1, which is divided by 20 contour lines with an equal increment. (b) Mach number contours. The large white region is a subsonic pocket. Velocity vectors in each of the four grids are displayed. Vectors on the innermost five shells near the compact object are omitted in order to avoid confusion. (c) As for (a) except $t=20$. (d) As for (b) except $t=20$.

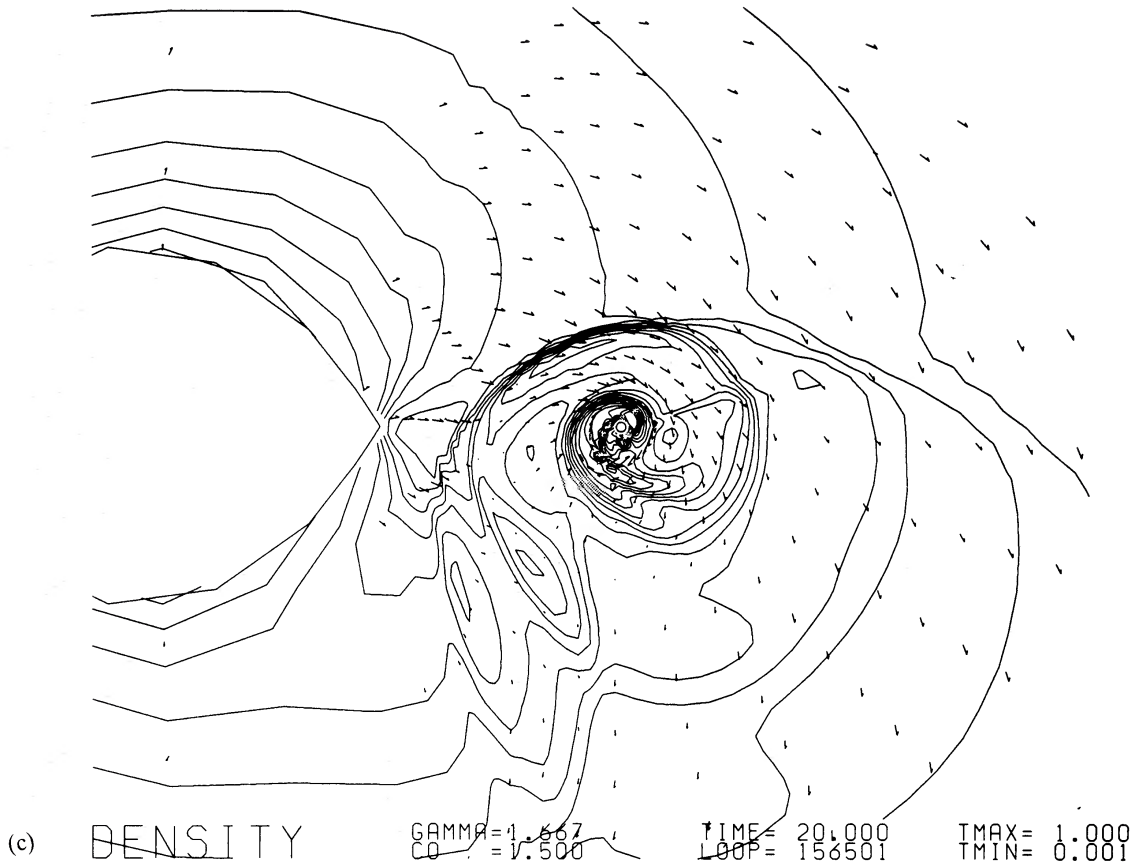

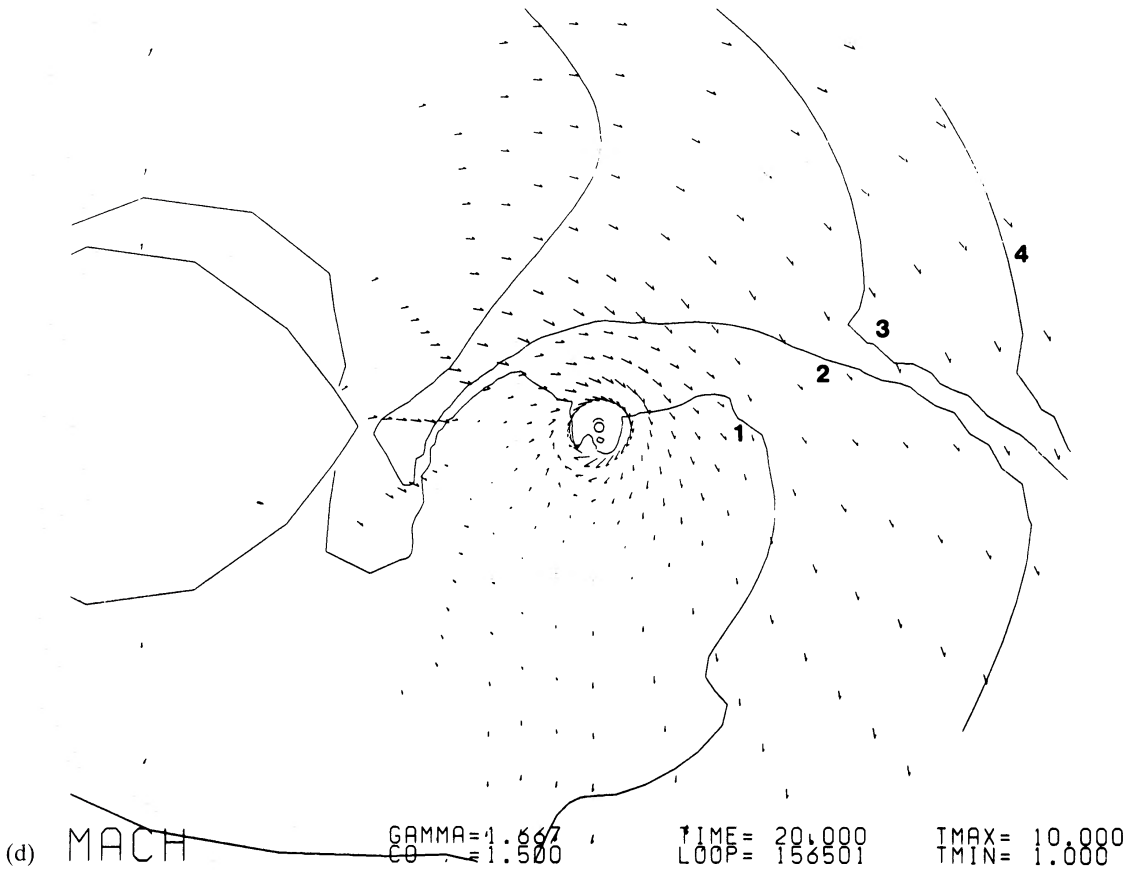

Figure 2 – *continued*

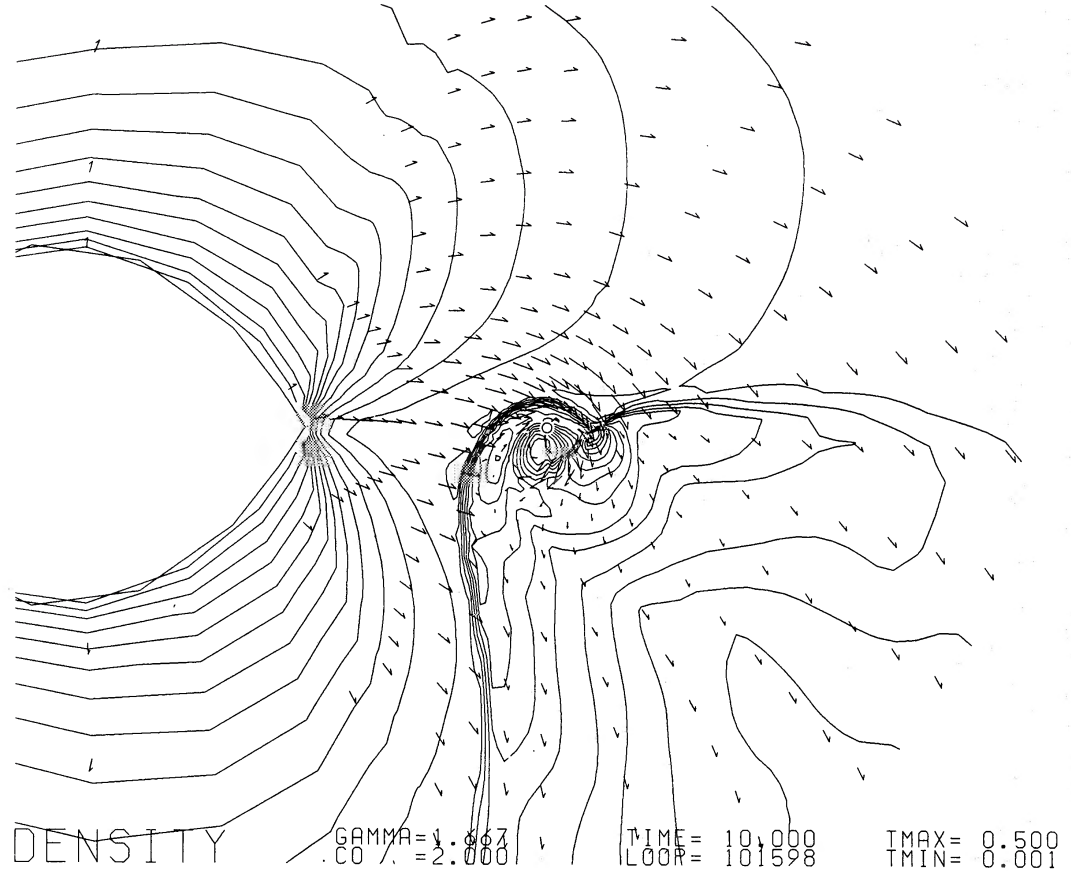

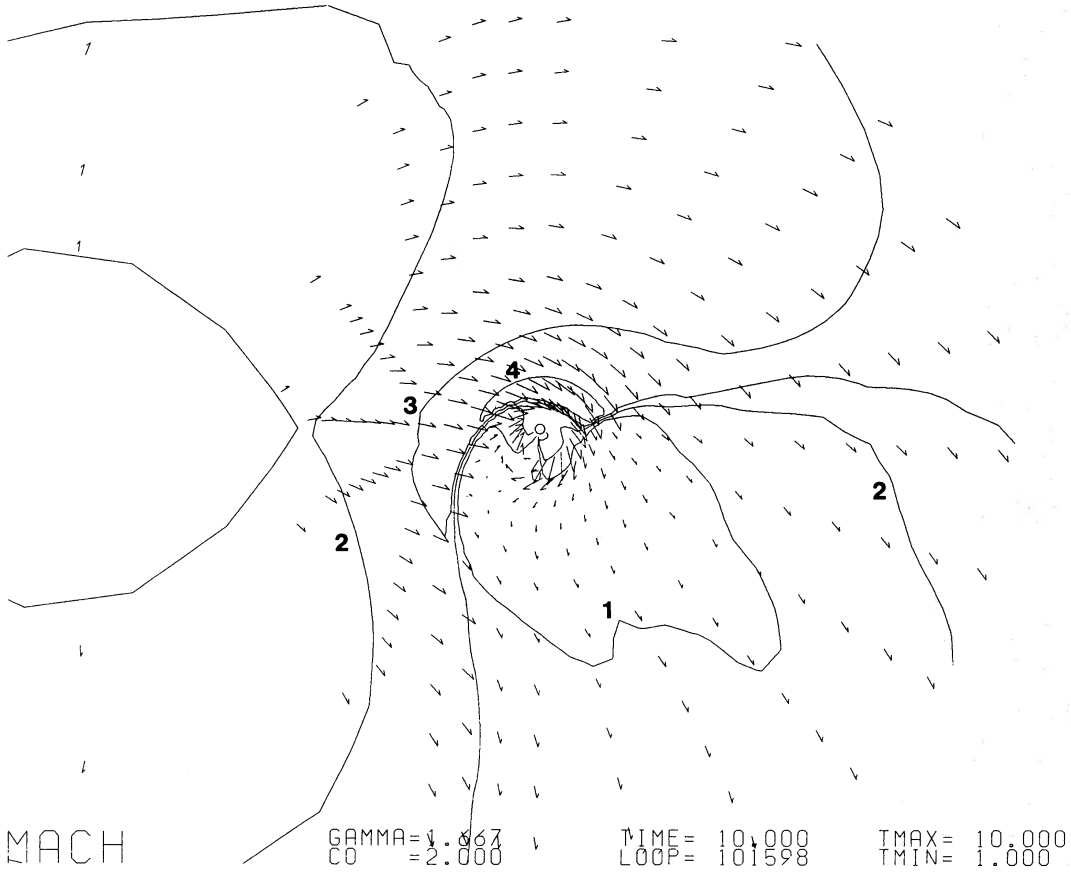

(b)

Figure 3. (a) Density contours for the model with $c_0=2.0$ and $\gamma=5/3$ at $t=10$. The density range is 0.001–0.5. (b) Mach number contours for the same model at $t=10$. (c) Density contours at $t=11$. (d) Mach number contours at $t=11$. (e) Density contours at $t=12$. (f) Mach number contours at $t=12$.

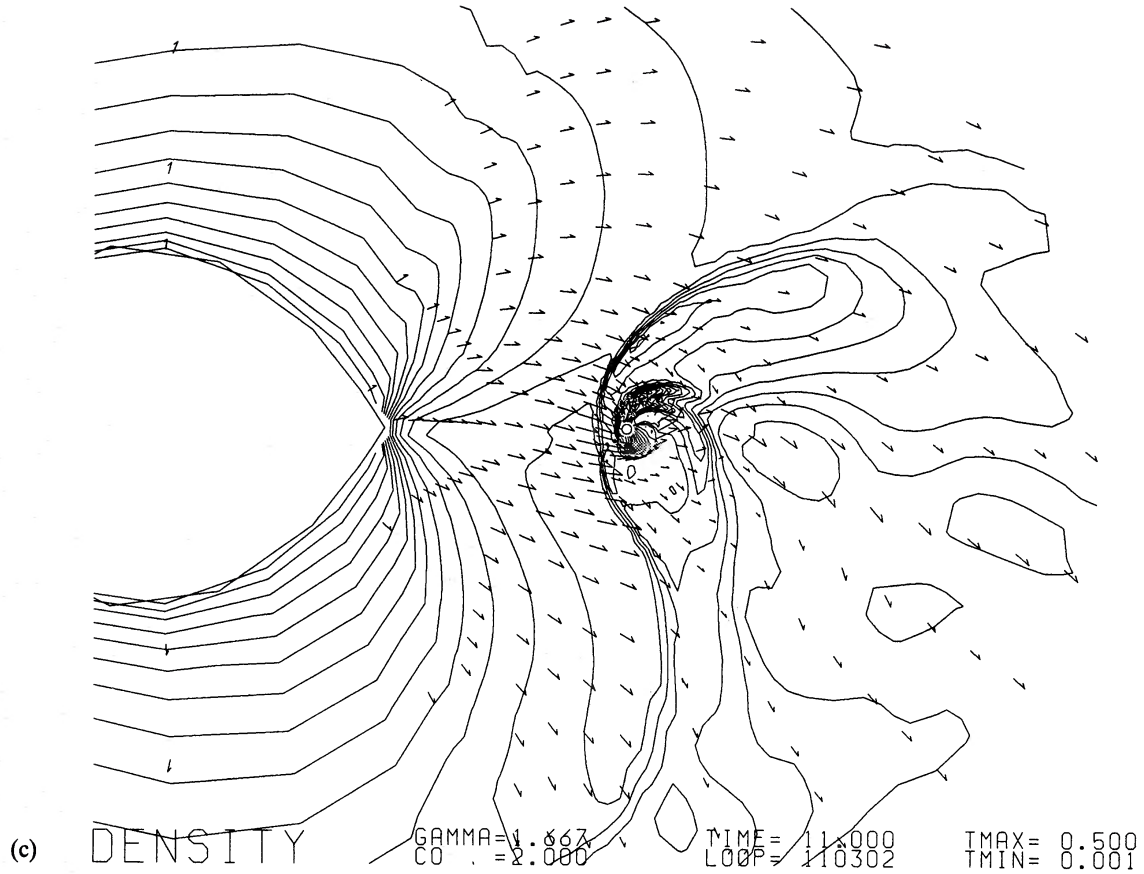

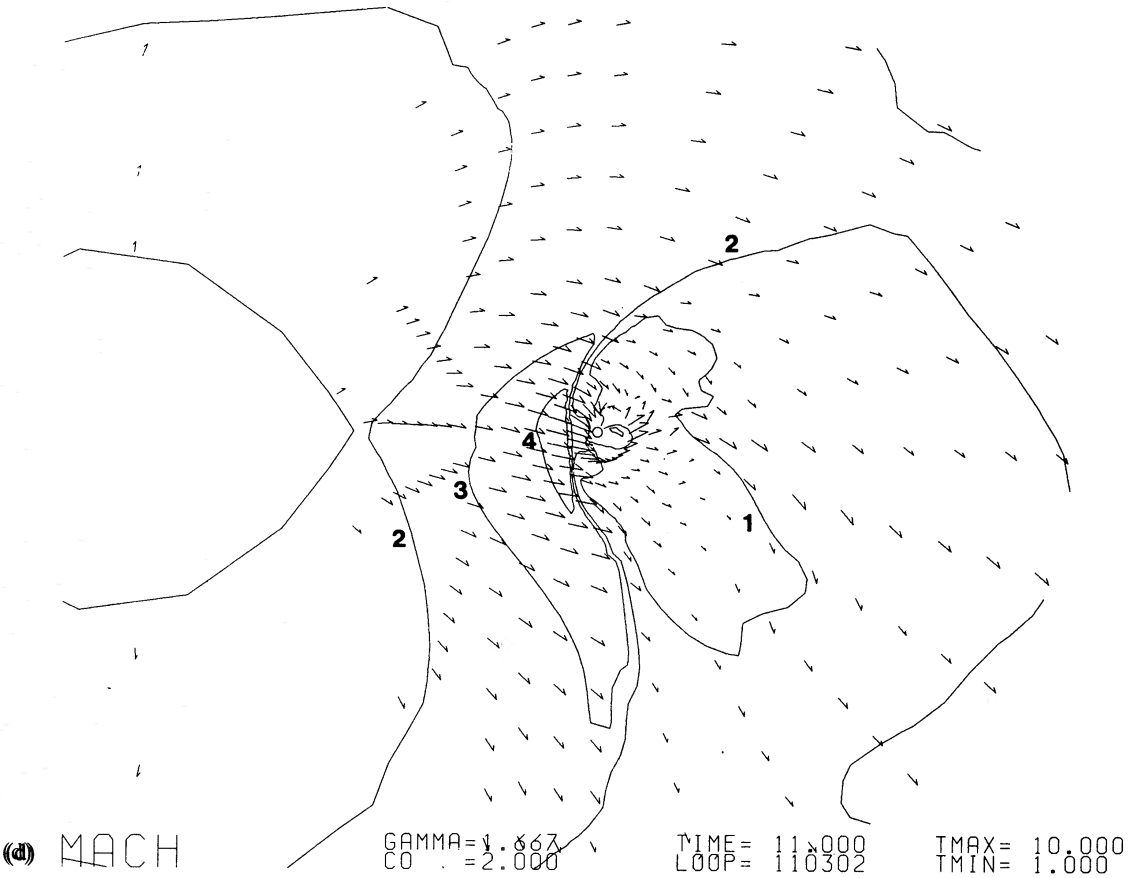

Figure 3 – *continued*

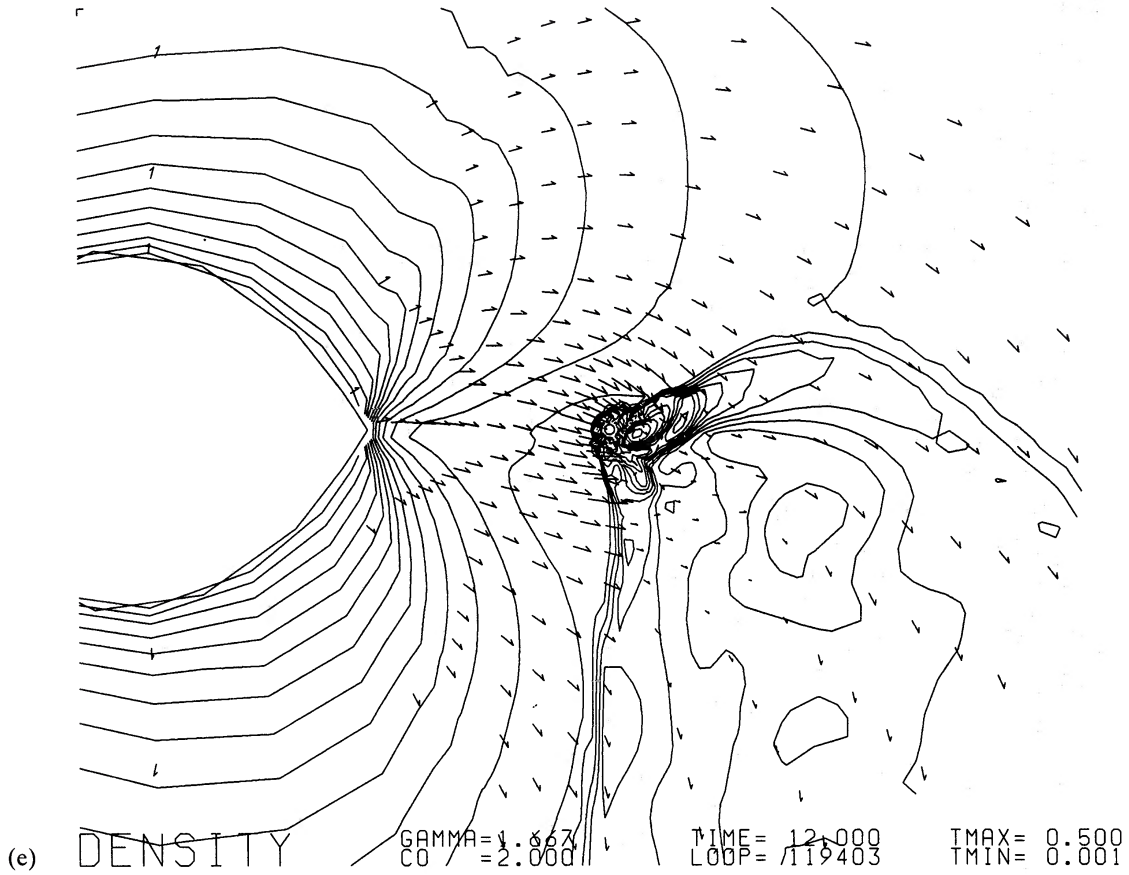

(e)

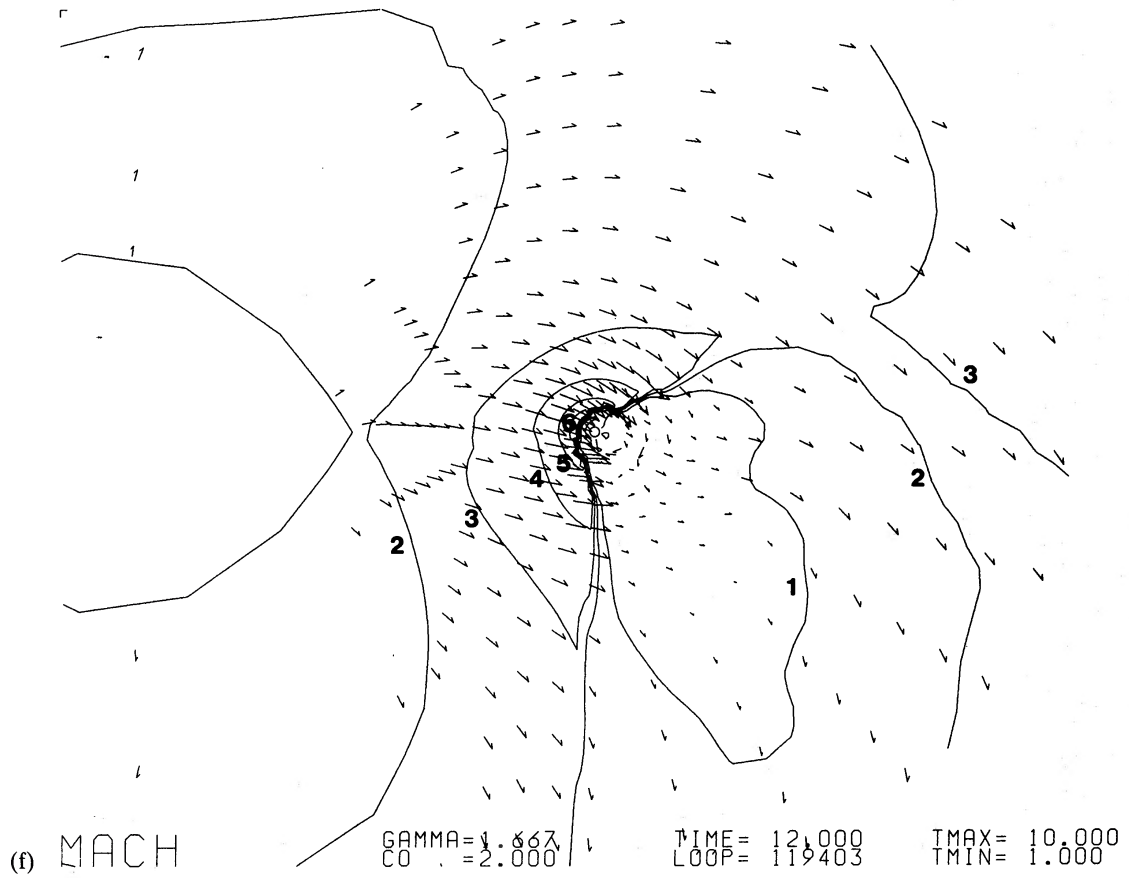

(f)

Figure 3–*continued*

This flip–flop nature is best illustrated by the time history of the angular momentum accretion rate, which not only oscillates heavily but also changes its sign sporadically. In Fig. 4, the mass-loss rate from the mass-losing star, $\dot{m}_l$, is shown by the solid line and the mass accretion rate, $\dot{m}_a$, on to the compact object by the dashed line. The latter quantity is made 10 times larger to show it clearly. The angular momentum accreted by the compact object in a unit time is monitored at the innermost shell, and is also shown in Fig. 4. It is computed on the rotating frame and is normalized by $(A\Omega)^2$.

3.4 STEADY CONICAL SHOCK

By the conical shock we mean a 2D cross-section of a conical shock, which is attached to the compact object. In the case of c_0=2.5, we have a rather steady conical shock. Fig. 5 shows a typical stage. This flow pattern is essentially the same as that obtained in Paper 1.

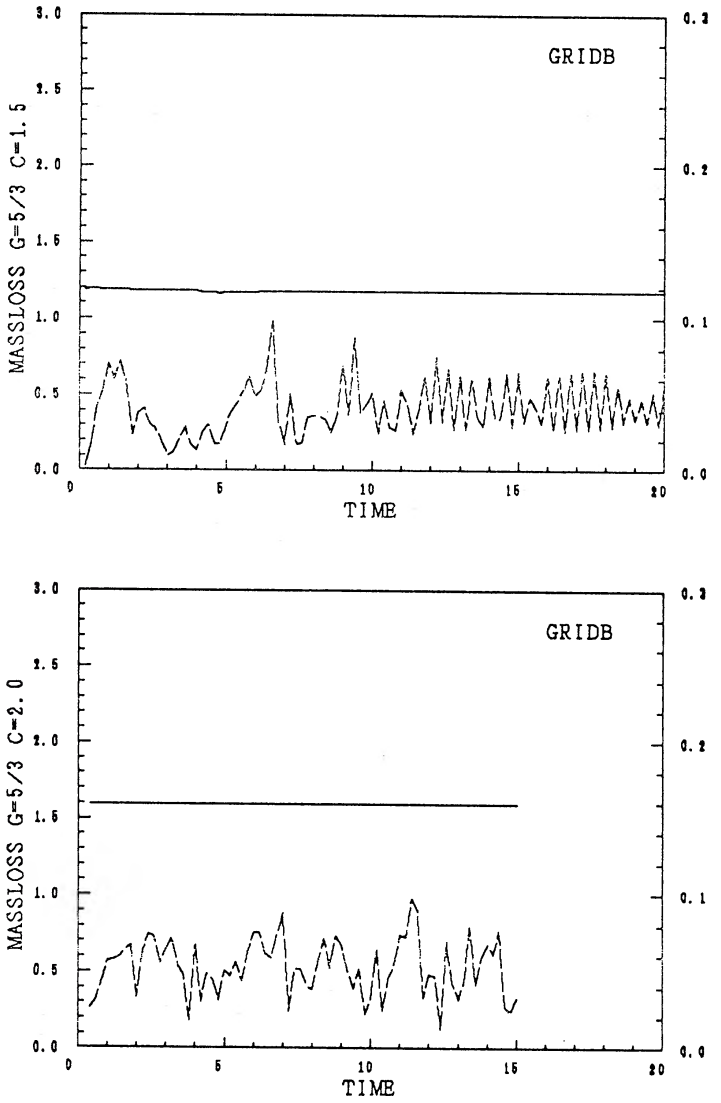

Figure 4. Time histories of the non-dimensional mass transfer rates and the non-dimensional specific angular momentum accreted by the compact object for the models with γ=5/3. The mass-loss rate from the mass-losing star is shown by the solid line and 10 times the mass-accretion rate on to the compact object by the dashed line. The time is made dimensionless by Ω^{-1}, and therefore 2π is an orbital period.

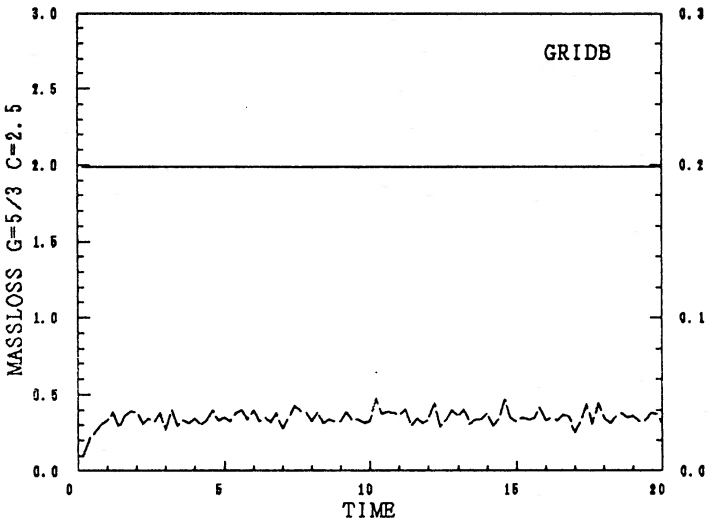

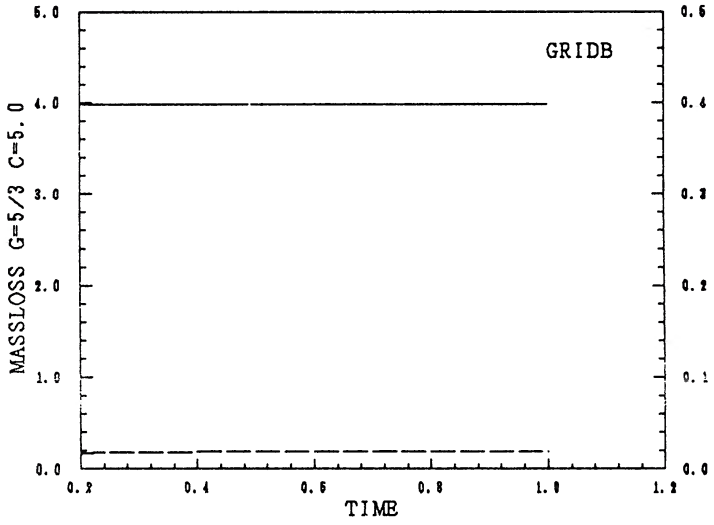

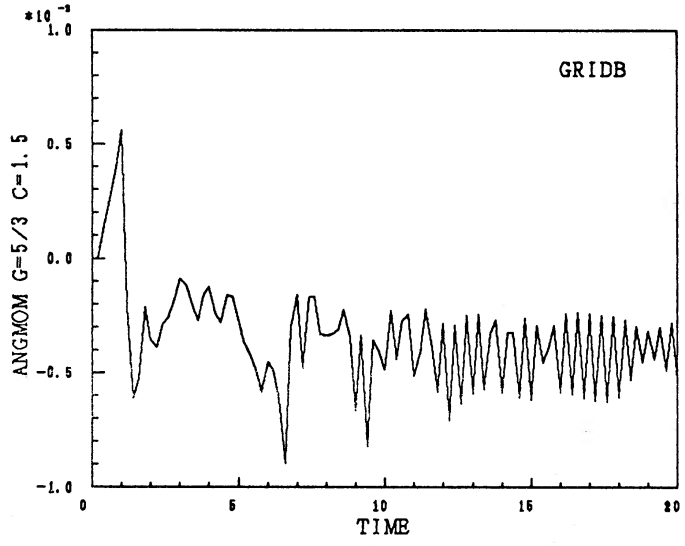

Figure 4 – *continued*

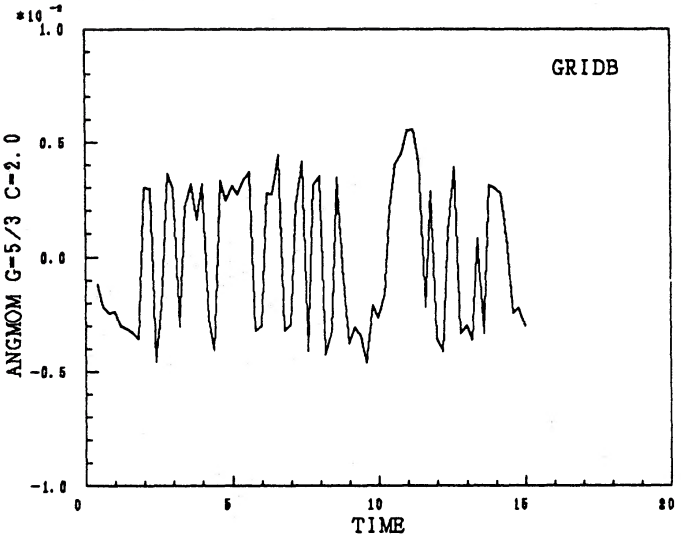

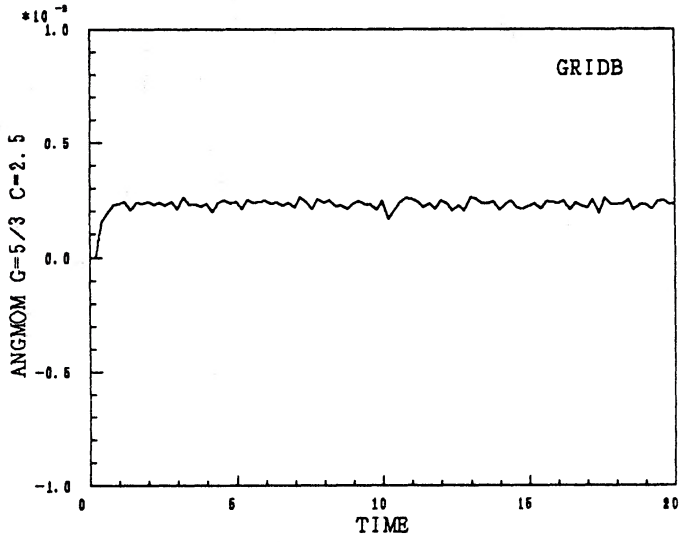

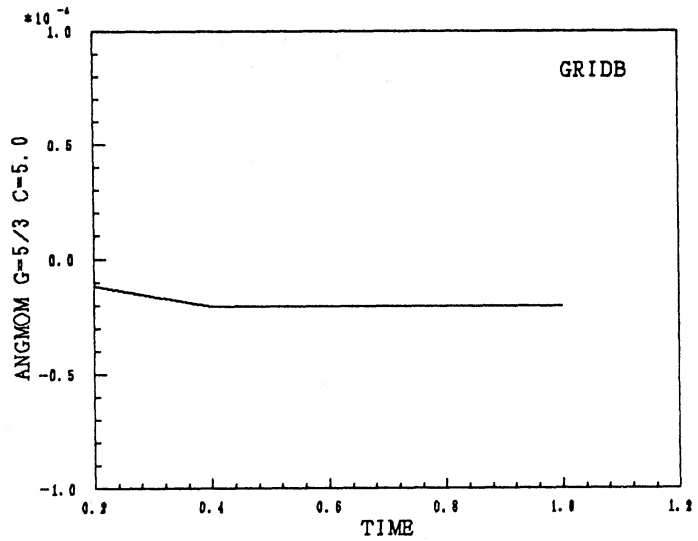

Figure 4 – *continued*

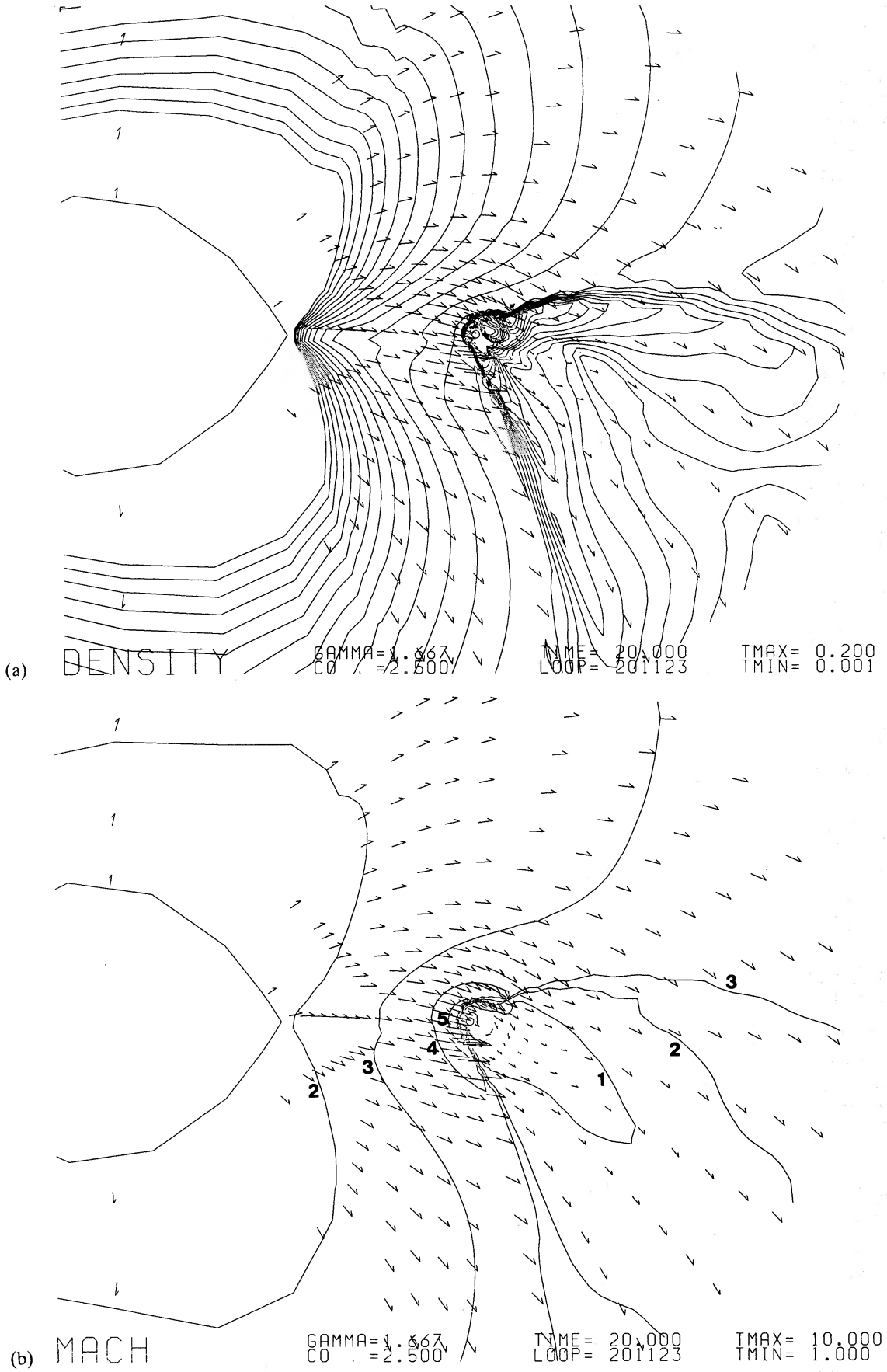

Figure 5. (a) Density contours, ranging from 0.001 to 0.2, of the model with $c_0=2.5$ and $\gamma=5/3$ at $t=20$. (b) Mach number contours and velocity vectors.

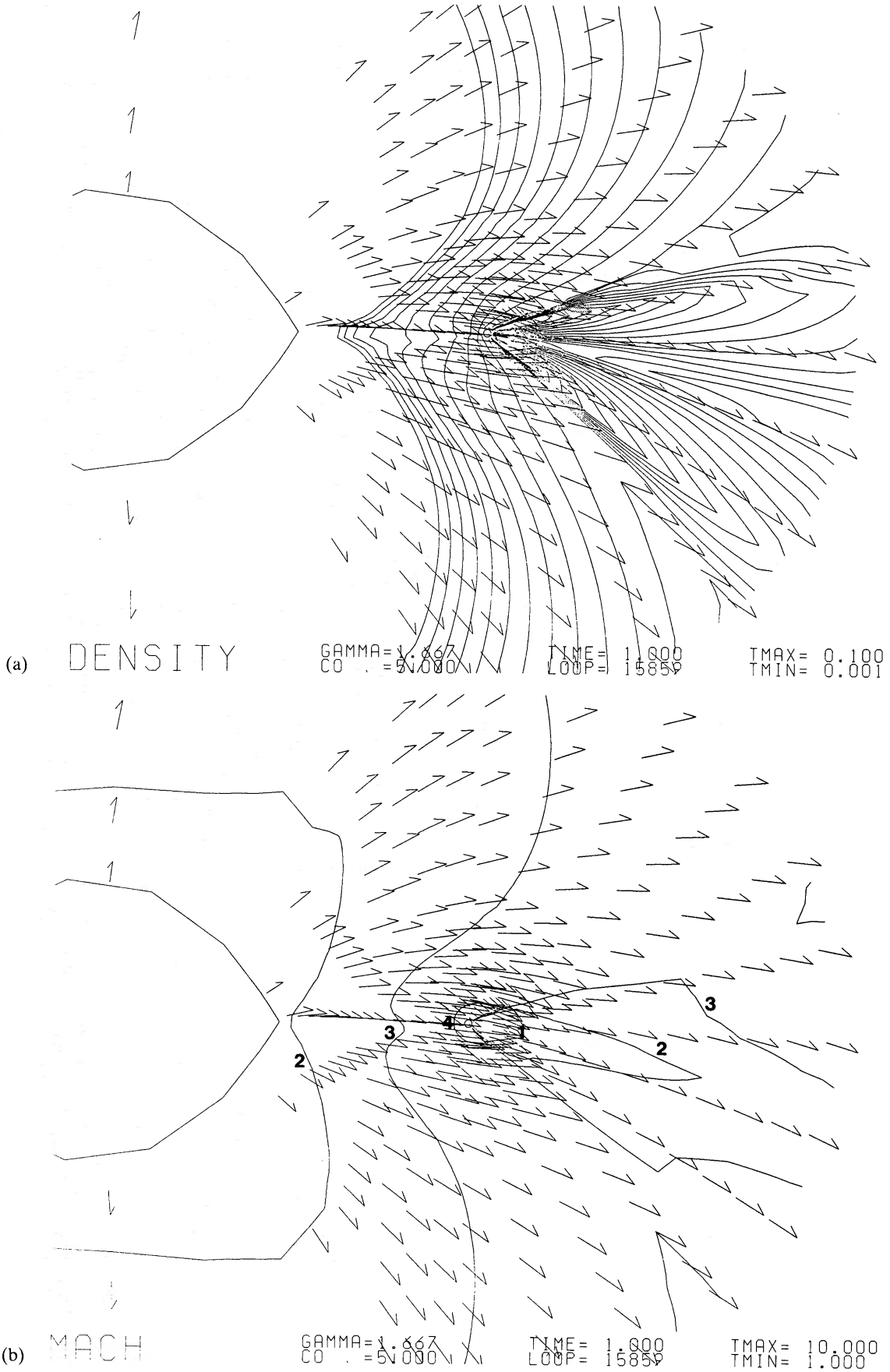

Figure 6. (a) Density contours of the model, ranging from 0.001 to 0.1, with c_0=5.0 and γ=5/3 at t=1. (b) Mach number contours and velocity vectors.

When we raise c_0 to 5.0, we have a very steady conical shock shown in Fig. 6. The mass accretion rate and the angular momentum accretion rate are also very steady as is shown in Fig. 4. Such an accretion flow is a typical one obtained in the axisymmetric calculation of the accretion (Shima *et al.* 1985).

3.4 NON-UNIQUE SOLUTIONS FOR LOWER WIND SPEED

A puzzling point is that the present result of the case $c_0=1.0$ using grid A shows a rotating disc with a spiral shock and is separated by a bow shock from a wind. This flow pattern is different from that in Paper 1, in which we had no bow shock. Then we recomputed the same model using grid B shown in Fig. 1. In this case we had a disc rotating clockwise, i.e. a retrograde-rotating disc! The bow shock is not steady. It emerges from the compact object, propagates towards the mass-losing star, disappears, and emerges again.

We guess that the flow pattern for low c_0 is very unstable and is sensitive to the slight variation of parameters, a numerical domain and a mesh size. In order to test this hypothesis, we computed the cases for $c_0=1.0$–1.4 using two grids shown in Fig. 1.

The results obtained using grid A are different to those using grid B. In grid A, we have an accretion disc surrounding the compact object for $c_0=1.0$ and 1.2. We can observe two spiral-shaped shock waves characteristic of an accretion disc in a Roche lobe overflow (Sawada, Matsuda & Hachisu 1986a, b; Sawada *et al.* 1987). We can also observe a bow shock separating the accretion disc from a wind gas. In the case of $c_0=1.3$ and 1.4, we have a retrograde-rotating disc with a bow shock and a conical shock, respectively. On the other hand, the corresponding results in grid B show a retrograde rotating disc having an unsteady bow shock for $c_0=1.0$–1.4.

Such a ridiculous situation can be understood in terms of the stand-off distance of the bow shock defined as the shortest distance from the compact object to the bow shock. The position of the bow shock is determined by a delicate balance of a wind pressure and a downstream pressure. In the present low wind speed range, the bow shock is very detached from the compact object and the stand–off distance is very large. Therefore, it is very sensitive to the choice of the grid, the boundary condition and even the initial condition in this parameter range.

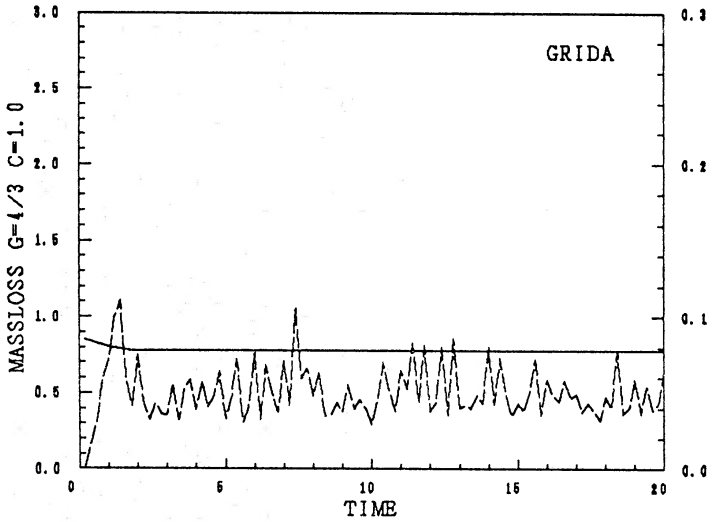

Figure 7. Time histories of the mass acretion rate and the angular momentum accretion rate for the model with $\gamma=4/3$.

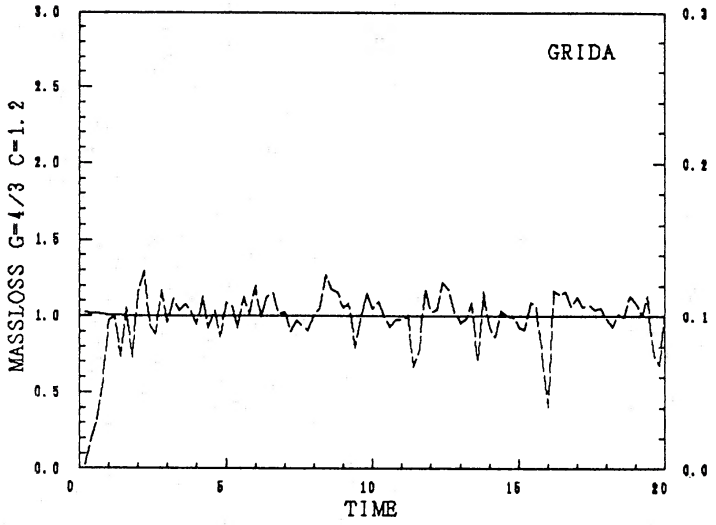

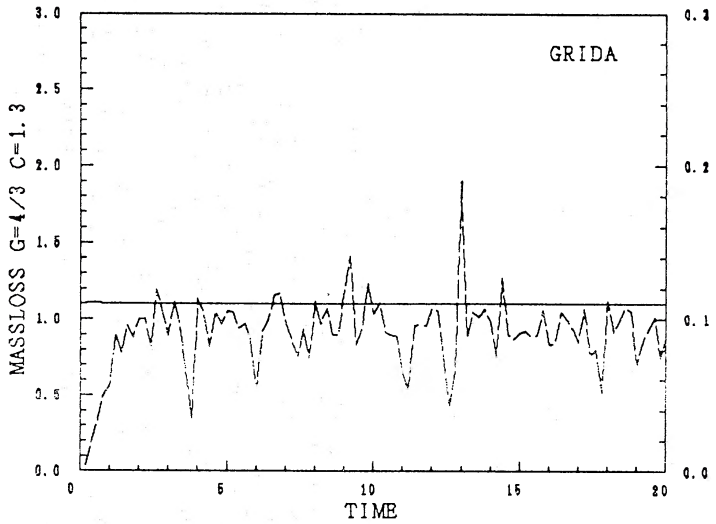

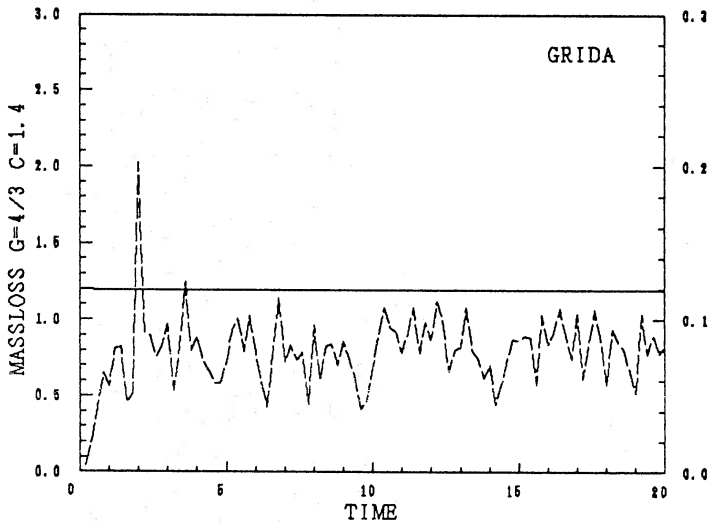

Figure 7–*continued*

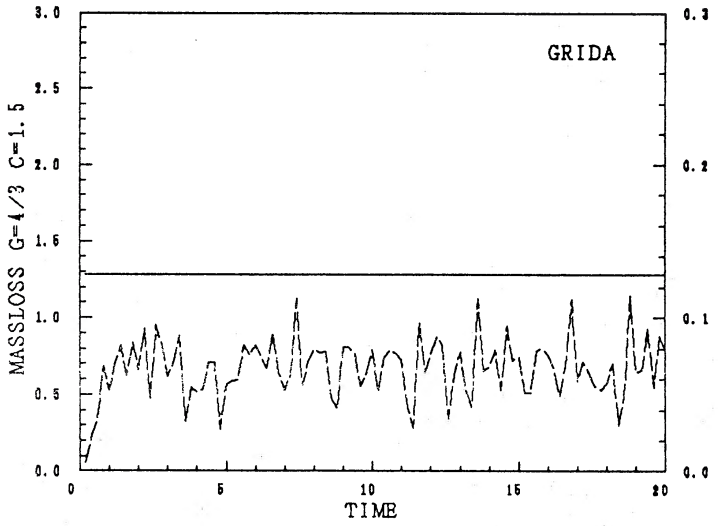

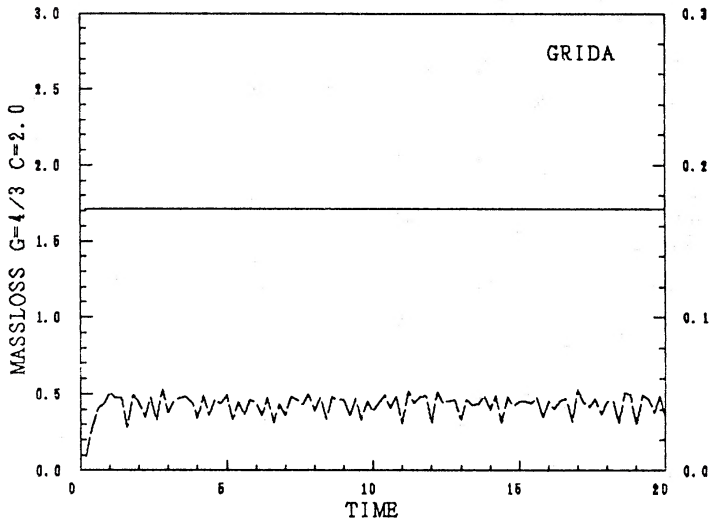

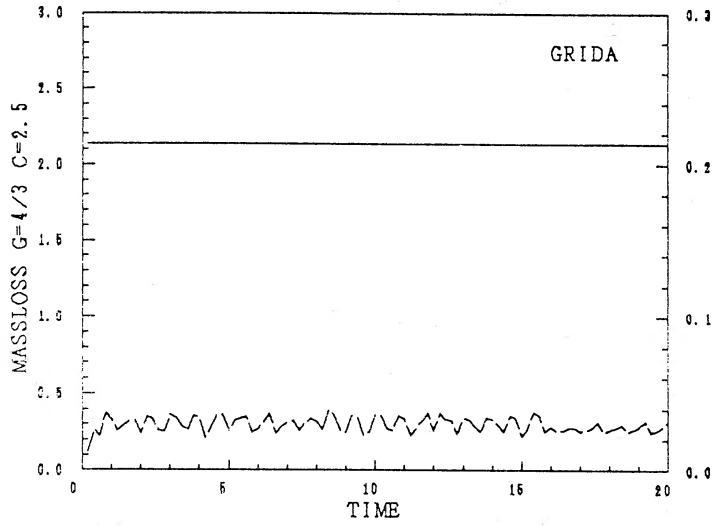

Figure 7–*continued*

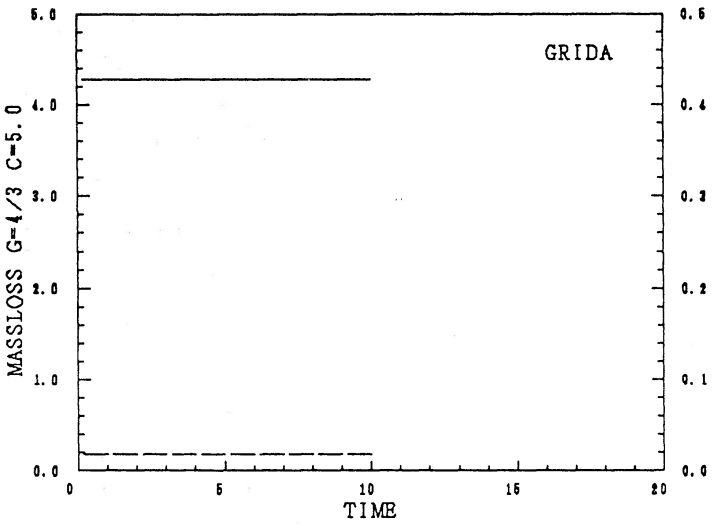

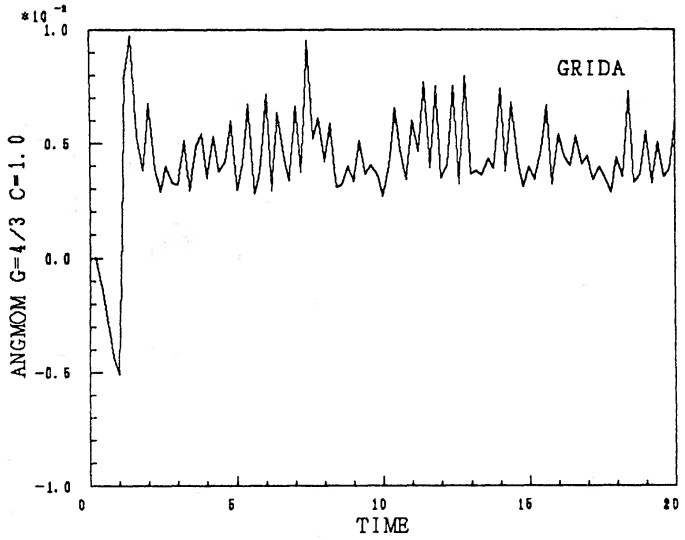

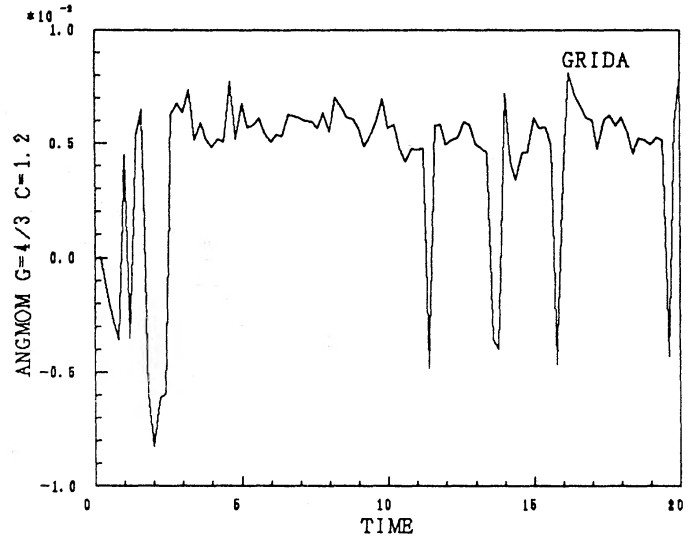

Figure 7–*continued*

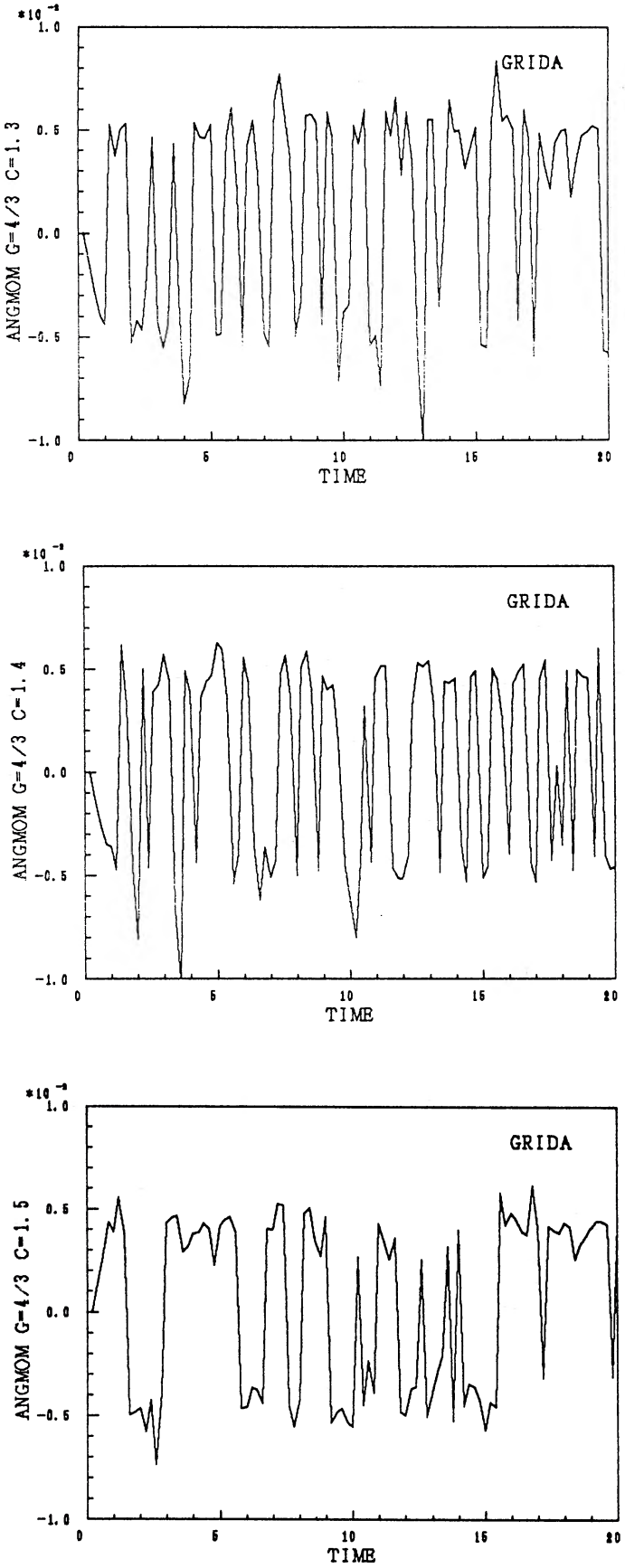

Figure 7–*continued*

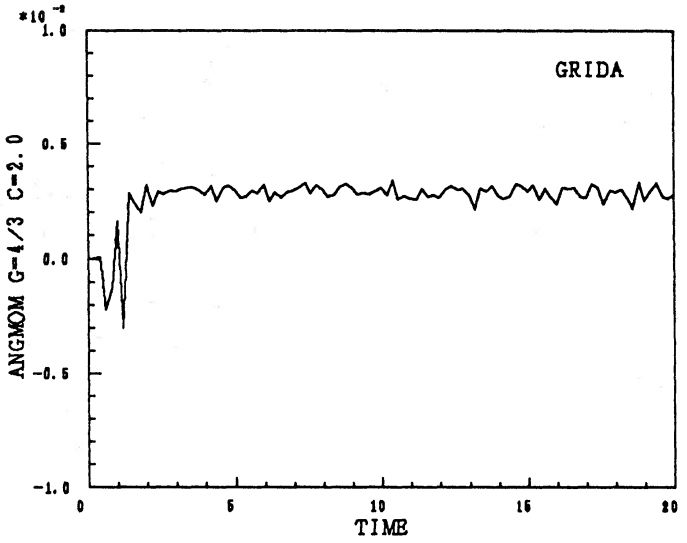

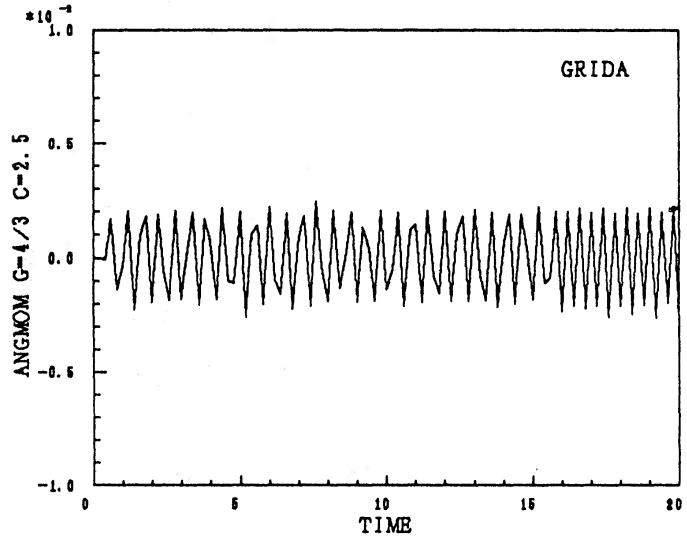

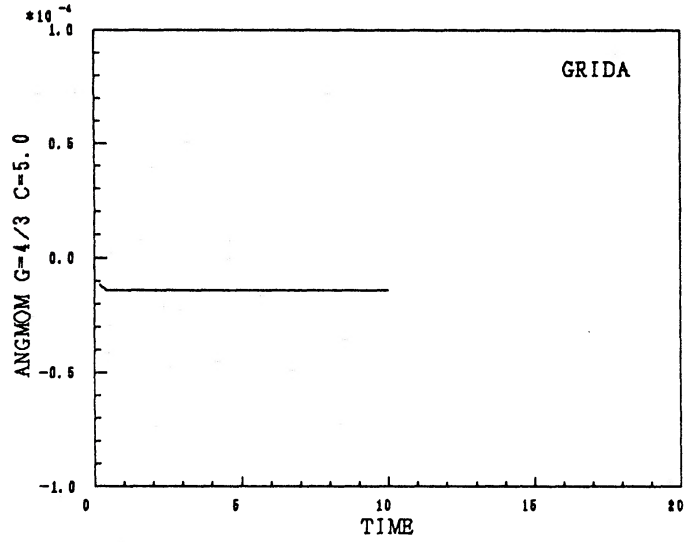

Figure 7–*continued*

We calculated an axisymmetric accretion flow on a compact object (see Shima *et al.* 1985). The Mach number at the upstream flow is fixed to be unity. In this case, the bow shock does not settle into a fixed position but propagates upstream, although there is a supersonic region close to the compact object. After the shock leaves the numerical domain, a new shock emerges. There is no steady flow. If the upstream Mach number is larger than unity, we would have a steady solution.

In our case, there is a subsonic region surrounding the mass-losing star, and therefore the shock entering into the subsonic region disappears. Therefore, we may not expect a steady flow in such a case.

The present bow shock has a large subsonic pocket behind it. When the subsonic region extends to the outer numerical boundary as is so in the present case, the flow may be influenced by the outer boundary condition.

We must conclude that the flow in this parameter range is very unstable and that no unique solution exists. A final solution sensitively depends on an initial state, boundary conditions, the

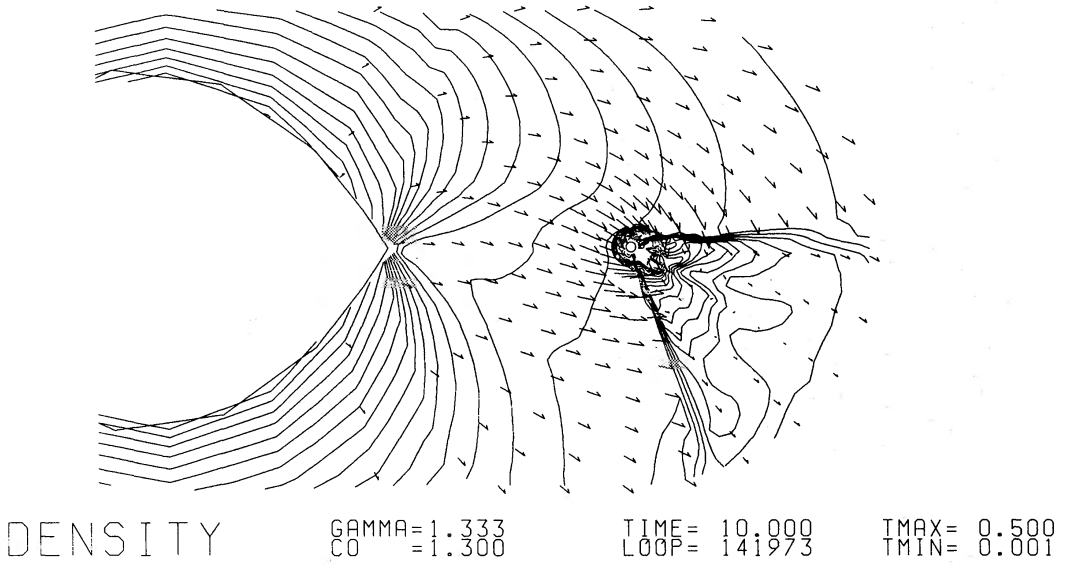

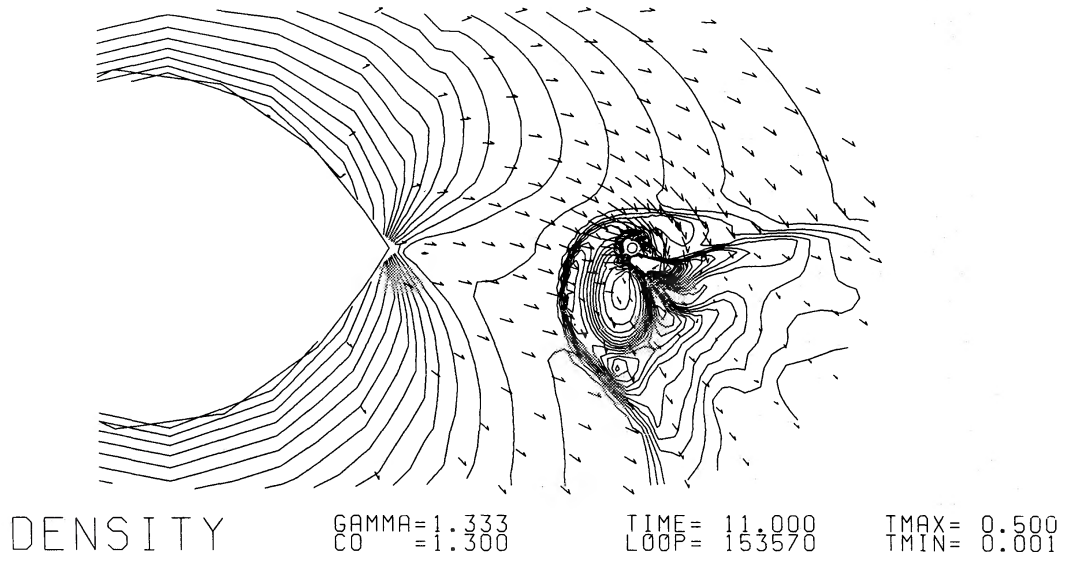

Figure 8. (a) Density contours of the model, ranging from 0.001 to 0.5, with $c_0=1.3$ and $\gamma=4/3$ at $t=10$. (b) Density contours at $t=11$.

grid used and a slight change of parameters. We do not give numerical results for C_0=1.0–1.4 here.

3.5 RESULTS FOR γ=4/3

We also computed the cases of γ=4/3. These cases are not so spectacular as the cases of γ=5/3. All cases except c_0=1.0 show conical shock patterns both on grid A and on grid B. Solutions are not steady in a strict sense, see, e.g. Fig. 7, where the mass accretion rate and the angular momentum accretion rate are shown. These solutions are based on grid A. Near solutions exhibit a flip–flop nature.

In Figs 8, 9 and 10, two typical density contours for two different times are shown for c_0=1.3, 1.4 and 2.5, respectively. Three major patterns of the oscillation of the conical shock are observed: (i) a spherical shock originating from the compact object propagates upstream (Fig. 8);

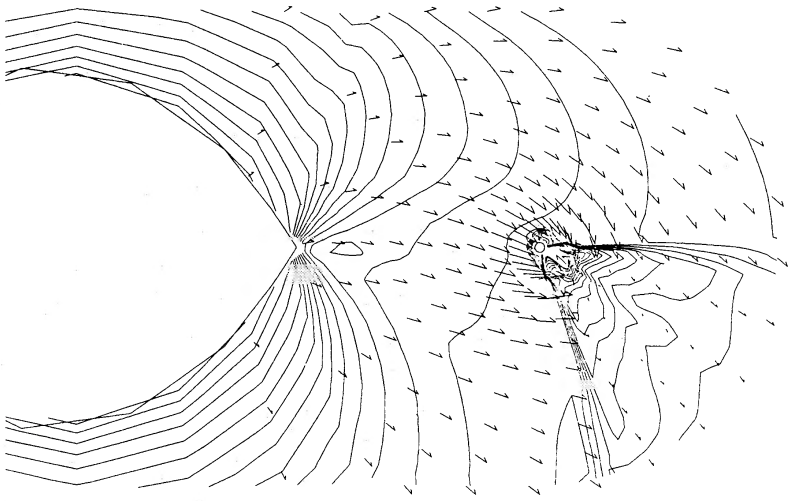

Figure 9. (a) Density contours of the model, ranging from 0.001 to 0.5, with c_0=1.4 and γ=4/3 at t=9. (b) Density contours at t=10.

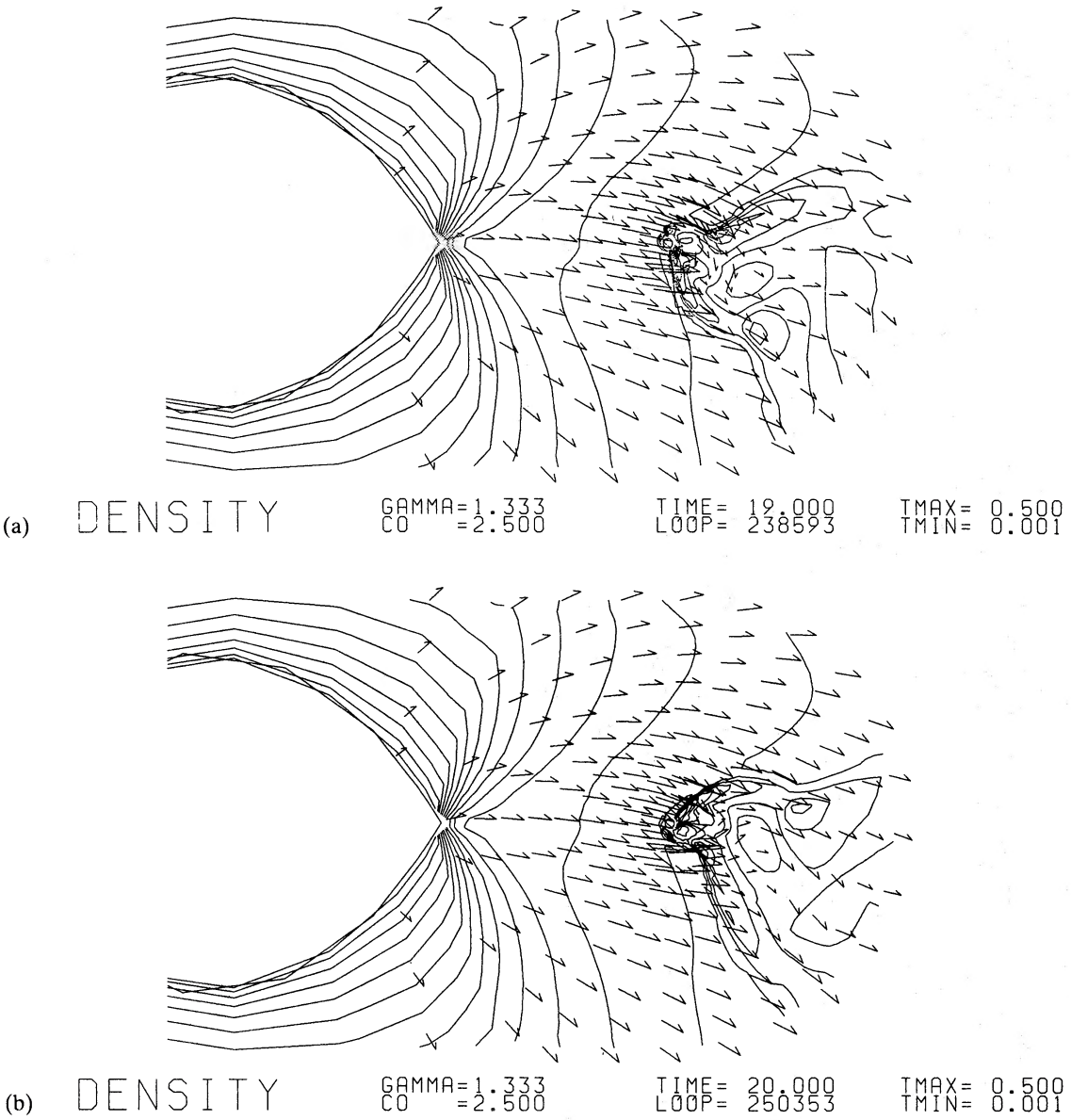

Figure 10. (a) Density contours of the model, ranging from 0.001 to 0.5, with $c_0=2.5$ and $\gamma=4/3$ at $t=19$. (b) Density contours at $t=20$.

(ii) a symmetric oscillation in which an opening angle of the shock changes with time (Fig. 9); (iii) asymmetric wavy motion perpendicular to the main flow direction (Fig. 10).

4 Angular momentum transfer

All models shown in the present work are summarized in Table 1. In the table, the mass accretion rate, $\dot{m}_a$, is a mean value. The accretion radius, r_a, is computed using the following relation rather than equation (1.1);

$$2r_a/2\pi A=\dot{m}_a/\dot{m}_0. \tag{4.1}$$

The accreted angular momentum is also a mean value. In the case of the flip–flow flow, values at two phases are shown.

Since we monitored the mass accretion rate, $\dot{m}_a$, and the angular momentum accretion rate, $\dot{L}$,

Table 1. Summary of calculated results. In the table, c_0 and γ represent the sound speed of gas at the surface of the mass-losing star and the ratio of specific heats, $\dot{m}_a$, $\dot{m}_l$ the dimensionless mass accretion rate and the mass loss rate, $\dot{L}$ the total angular momentum accretion rate, r_a the accretion radius, l the specific angular momentum, and η the efficiency factor, respectively.

γ	C_0	$\dot{m}_a/\dot{m}_l$	$\dot{L}$	r_a	$l=L/\dot{m}_a$	η
5/3	1.5	0.033	−0.004	0.104	0.100	−18.49
	2.0	0.031	−0.004~0.003	0.097	−0.080~0.060	−17.00~12.75
	2.5	0.015	0.002	0.047	0.067	60.66
	5.0	0.005	−0.00002	0.016	0.001	8.11
4/3	1.0	0.063	0.005	0.195	0.125	6.57
	1.2	0.100	−0.004~0.006	0.314	−0.040~0.060	−0.81~1.68
	1.3	0.082	−0.006~0.005	0.258	−0.067~0.056	−2.01~1.68
	1.4	0.067	−0.005~0.005	0.210	−0.063~0.063	−2.86~2.86
	1.5	0.055	−0.005~0.004	0.173	−0.083~0.067	−5.55~4.48
	2.0	0.024	0.003	0.075	0.075	26.67
	2.5	0.014	−0.002~0.002	0.044	−0.067~0.067	−69.21~69.21
	5.0	0.005	−0.000014	0.016	0.0007	5.47

we can compute the specific angular momentum, l, carried by the accreting gas using a following formula:

$$l=\dot{L}/\dot{m}_a. \tag{4.2}$$

Not surprisingly we obtained $l\sim\pm0.1$ for cases with a disc, since a gas particle undergoes nearly Keplerian motion about the compact object. Here l is normalized by $A^2\Omega$.

We can formally compute η based on the above l, and we obtain a rather large absolute value of η. This value has no significant meaning, since it depends on the size of the inner numerical boundary. In the cases of conical shock, the calculated efficiency factor η may have some meaning. It should be noted that the absolute values of the efficiency factor η obtained in the present calculation are generally larger than unity.

5 Conclusion and discussion

5.1 CONCLUSION

We can draw the following conclusions:

(i) One can see that the absolute values of η obtained in our calculations are fairly large, and that they are certainly larger than the values quoted by Livio *et al.* (1986), Soker *et al.* (1986) and Anzer *et al.* (1987). It seems that our results do not support Davies & Pringle's theory (1980).

(ii) The accreted angular momentum can become negative. This is not the case in Shapiro & Lightman's theory. Wang (1981) argued that η may become negative if the boundary condition on the mass-losing star has azimuthal dependence. Our result is not the same as his, since the boundary condition on the surface of the mass-losing star is assumed uniform.

(iii) The accreted angular momentum changes its sign sporadically for flip–flop flows. This effect may explain the period fluctuation of Vela X-1 discussed in the introduction.

(iv) We have a conical accretion shock for $\gamma=5/3$ and $c_0>=2.5$. The cases for $\gamma=4/3$ show a conical shock except for $c_0=1.0$. In the case of $\gamma=5/3$ and $c_0=1.5$, we have a retrograde rotating disc bounded by a bow shock from a wind gas.

5.2 UNSTEADY FLOW

A characteristic nature of our flow is the unsteadiness for almost all models. It may be argued that a small oscillation of a flow and a flip–flop are induced by an improper choice of numerical

boundary conditions. However, as can be seen in Fig. 4, the boundary condition at the surface of the mass-losing star is very steady.

It may be difficult to determine the boundary condition at the downstream end, if the gas flows out subsonically. This is because a numerical perturbation may be reflected back at the outflow boundary into a main flow field. In numerical experiments of axisymmetric jets, Ishii & Umeda (1986) and Matsuda *et al.* (1987) found that an improper choice of boundary conditions enhances the oscillatory motion. They reported that the Sawada's boundary condition or the ambient gas condition (Sawada *et al.* 1986c) used in the present work gives the most satisfactory result.

In this boundary condition, numerical flux on the downstream boundary are computed by solving a Riemann problem between the state just upstream and the fixed state out of the boundary. By choosing the fixed state so that only one characteristic wave, say $u-c$, enters a numerical domain in a case of subsonic outflow, the external effect can be minimized. If the outflow is supersonic, all characteristic waves go out of the numerical region, and no effect outside the region is felt.

Even if we insist that our boundary condition is a proper one, the possibility cannot be ruled out that the outer boundary condition affects the result. This is probably the case in our models for low sound speeds. However, in the cases of the flip–flop flows, the Mach number at the outer boundary is larger than unity, which means that the outer boundary cannot have any effect on the upstream flow. Taking this into consideration, we conclude that the unsteady nature of our flows is a physical one rather than numerical one.

The oscillation of the conical shock discussed before may be caused by a propagation of pressure waves in the subsonic pocket at the downstream side of the shock. Such a phenomenon is sometimes observed on the wings of transonic aircraft. Assuming the sound velocity in the subsonic pocket to be of the order of unity and taking the typical length as the accretion radius, which ranges from about 0.01 to 0.1, the propagation time of the disturbance is about 0.01–0.1. This value is consistent with the transition time in the flip–flop shown in Figs 4 and 7.

5.3 DISCREPANCY BETWEEN OUR RESULTS AND OTHERS

Our results do not support Davies & Pringle's theory. This is not surprising because Davies & Pringle's results were derived in the case of infinite Mach number, in which line accretion results. On the other hand, rather low Mach number cases are considered in our calculation, and a pressure effect is important behind the bow shock. Moreover, all assumptions made by Davies & Pringle, i.e. a point-like star, an accretion line pointing to the star, and no dissipation, are not satisfied in our result.

Our results do not coincide with numerical simulations by other authors (Livio *et al.* 1986; Soker *et al.* 1986; Anzer *et al.* 1987), who support Davies & Pringle's theory. What are the causes of this discrepancy? These authors assumed a parallel flow having non-uniform density far-upstream, while we computed a flow with a more realistic configuration. Their Mach number is constant in the upstream region, while ours varies from place to place. This is particularly important in deciding the shock position for low Mach number cases.

They computed the pressureless case (Livio *et al.* 1986) or isothermal case (Soker *et al.* 1986; Anzer *et al.* 1987). If γ is 5/3, the stand-off distance of the bow shock is large in low Mach number cases. In such instances we have an accretion disc bounded by a detached bow shock.

Our solutions are unsteady, while other authors claim that they obtained steady solutions. In our experience of numerical simulations of jets (Matsuda *et al.* 1987) an unsteady flow develops when artificial/numerical viscosity is reduced by increasing the number of meshes. A seemingly steady solution occurs either if a rather coarse mesh is adopted or too much artificial viscosity is included.

In our calculation a stream in an accretion column does not point to the mass-accreting star. Gas particles in the stream are accreted through a dissipation in spiral shocks, if they exist. These spiral shocks are produced because of the tidal effects of the companion star. These tidal effects are not taken into account in the numerical calculations quoted above. A finite size of our mass-accreting star may contribute somehow. We have taken into account the effects of the Coriolis force, which becomes important for a low-velocity wind, and which other authors have ignored.

All these effects mentioned above result in a discrepancy between our results and others. If these are the only reasons for the discrepancy then there may not be any contradiction among them. In any rate we need further investigation to settle the problem.

Acknowledgments

The authors thank Professor T. Sakurai of Kyoto University and Mr E. Shima of Kawasaki heavy industries for their useful discussions. TM thanks Professor F. Nagase and Dr K. Masai of Nagoya University, and Professor K. Makishima of University of Tokyo for their stimulating discussions and useful information. He also acknowledges Dr U. Anzer for sending a preprint and valuable comments.

The computations were performed on the Fujitsu (FACOM) VP200 vector processor at the data processing centre of Kyoto University, and also on the Fujitsu VP50 at the Nobeyama Radio Observatory. This work was supported by the Grant-in-Aid for Scientific Research (61540183) of the Ministry of Education, Science and Culture in Japan.

References

Anzer, U., Börner, G. & Monaghan, J. J., 1987. *Astr. Astrophys.*, in press.
Biermann, P., 1971. *Astr. Astrophys.*, **10,** 205.
Boynton, E. P., Deeter, J. E., Lamb, F. K., Zylstra, G., Pravdo, S. H., White, N. E., Wood, K. S. & Yentis, D. J., 1984. *Astrophys. J.*, **283,** L53.
Davidson, K. & Ostriker, J. P., 1973. *Astrophys. J.*, **179,** 585.
Davies, R. E. & Pringle, J. E., 1980. *Mon. Not. R. astr. Soc.*, **191,** 599.
Gingold, R. A. & Monaghan, J. J., 1983. *Mon. Not. R. astr. Soc.*, **204,** 715.
Henrichs, H. F., 1983. *Accretion-driven Stellar X-ray Sources,* eds Lewin, W. H. G. & van den Heuvel, P. J., Cambridge University Press.
Ishii, R. & Umeda, Y., 1986. *AIAA Paper 86–1371.*
Livio, M., Soker, N., de Kool, M. & Savonije, G. J., 1986. *Mon. Not. R. astr. Soc.*, **218,** 593.
Makishima, K., Koyama, K., Hayakawa, S. & Nagase, F., 1986. *ISAS Research Note RN 321.*
Matsuda, T., Umeda, Y., Ishii, R., Yasuda, M. & Sawada, K., 1987. *Mem. Fac. Eng. Kyoto Univ.*, **49,** 83.
Nagase, F., 1981. *Space Sci. Rev.*, **30,** 395.
Nagase, F. *et al.*, 1984. *Astrophys. J.*, **280,** 259.
Rappaport, S. A. & Joss, P. C., 1983. *Accretion-driven Stellar X-ray Sources,* eds Lewin, W. H. G. & van den Heuvel, P. J., Cambridge University Press.
Sawada, K., Matsuda, T. & Hachisu, I., 1986a. *Mon. Not. R. astr. Soc.*, **219,** 75.
Sawada, K., Matsuda, T. & Hachisu, I., 1986b. *Mon. Not. R. astr. Soc.*, **221,** 687.
Sawada, K., Shima, E., Matsuda, T. & Inaguchi, T., 1986c. *Mem. Fac. Eng. Kyoto Univ.*, **48,** 240.
Sawada, K., Matsuda, T., Inoue, M. & Hachisu, I., 1987. *Mon. Not. R. astr. Soc.*, **224,** 307.
Shapiro, S. L. & Lightman, A. P., 1976. *Astrophys. J.*, **204,** 555.
Shima, E., Matsuda, T., Takeda, H. & Sawada, K., 1985. *Mon. Not. R. astr. Soc.*, **217,** 367.
Soker, N., Livio, M., de Kool, M. & Savonije, G. J., 1986. *Mon. Not. R. astr. Soc.*, **221,** 445.
Sorensen, S.-A., Matsuda, T. & Sakurai, T., 1975. *Astrophys. Space Sci.*, **33,** 465.
Wang, Y.-M., 1981. *Astr. Astrophys.*, **102,** 36.